First-Principles Studies of the Activation of Oxygen Molecule and Its Role in Partial Oxidation of Methane on Boron-Doped Single-Walled Carbon Nanotubes

ARTICLE *in* THE JOURNAL OF PHYSICAL CHEMISTRY C · AUGUST 2013

Impact Factor: 4.77 · DOI: 10.1021/jp404079j

2 AUTHORS:

Bo Li
Chinese Academy of Sciences
25 PUBLICATIONS **255** CITATIONS
SEE PROFILE

Dangsheng Su
Chinese Academy of Sciences
643 PUBLICATIONS **13,139** CITATIONS
SEE PROFILE

THE JOURNAL OF PHYSICAL CHEMISTRY C

Article

pubs.acs.org/JPCC

First-Principles Studies of the Activation of Oxygen Molecule and Its Role in Partial Oxidation of Methane on Boron-Doped Single-Walled Carbon Nanotubes

Bo Li and Dangsheng Su*

Shenyang National Laboratory for Materials Science, Institute of Metal Research, Chinese Academy of Sciences, 72 Wenhua Road, Shenyang 110016, China

ABSTRACT: The nanostructured carbon materials have been widely tested as catalyst in a number of chemical reactions. The oxygen functional groups on nanostructured carbon catalyst are believed to be the active sites, for example, in the oxidative dehydrogenation reaction of hydrocarbons. However, the doping is one of the effective ways to tune the properties of nanostructured carbon materials. It will be important to examine the effect of doping on the catalytic properties of oxygen molecule on nanostructured carbon materials. In current work, the dissociation of the oxygen molecule on the boron-doped single-walled carbon nanotube (BSWCNT) and their catalytic properties in the partial oxidation of methane to formaldehyde are investigated by using first-principles calculations. Both defect-free BSWCNT and defective BSWCNT with a monovacancy are studied, and the comparisons between them are made. BSWCNT demonstrates a good ability for the dissociation of oxygen molecule. The favorable binding sites for the dissociated oxygen molecule are the positively charged atoms on BSWCNTs because oxygen molecule itself is negatively charged by obtaining electrons from carbons. The barrier of the oxygen dissociation is 0.88 and 0.12 eV, respectively, for defect-free and defective BSWCNTs. Furthermore, the dissociated oxygen molecule on BSWCNT exhibits the ability to break the C−H bond in methane molecule and the dissociated fragments (CH_3 and H) bind on the oxygens on BSWCNTs. The C−H bond breaking results from the charge abstraction from hydrogen in methane molecule by BSWCNT. The minimum energy path looks similar for both defect-free and defective BSWCNTs, which involves a methyl radical translation after transition state. However, the barrier is smaller by 0.5 eV on defective BSWCNTs and comparable with other catalysts for methane activation. The CH_3O on BSWCNT can be further converted to the formaldehyde with the calculated barrier of 1.37 eV. The current study indicates that the boron doping is a promising effective way to optimize the catalytic properties of carbon nanotube catalyst.

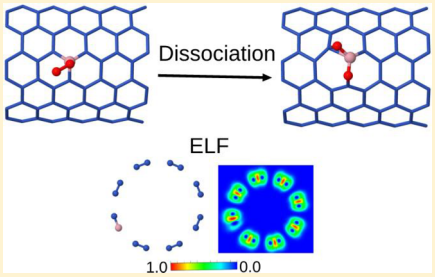

1. INTRODUCTION

The nanostructured carbon materials like nanotube (CNT),[1] nanofiber,[2,3] nanodiamond,[4] and graphene[5] have become an important class of the heterogeneous catalyst, which have been applied in various chemical reactions. One of the most widely studied reactions for nanostructured carbon catalyst is the oxidative dehydrogenation reaction (ODH) of hydrocarbons, which has been tested for ethane,[6] propane,[3,7,8] butane,[9−11] and ethlybenzene.[12−15] In particular, the surface-modified CNT catalyst shows the better performance than the well-known metal oxide catalyst V/MgO in the ODH of butane.[9] This study opened the possibility to replace the metal-based catalyst with the nanostructured carbon materials and achieved so-called metal-free catalyst.[16,17] However, the catalytic performance for the ODH of ethane and propane is modest due to their strong stability and the higher reaction temperatures.[18] There are much room for the further improvements for nanostructured carbon catalysts in these reactions compared with the counterpart of the metal oxide catalysts. It is widely accepted that the oxygen functional groups on nanostructured carbon catalyst are the active sites in the ODH.[1,9,13,19] It is clear that further advances for nanostructured carbon catalyst in ODH reactions rely on the optimization of catalytic properties of oxygen groups.

One of the possible ways to tailor the properties of nanostructured carbon material is the heteroatom doping, which means to introduce the alien atoms other than carbon into the carbon matrix. Among various heteroatoms, boron is an important dopant for carbon materials, which have been used in various fields such as superconductivity,[20] catalysis,[21] gas sensor,[22,23] hydrogen storage.[24,25] Yang et al. demonstrated that the boron-doped CNT is a much better oxygen reduction reaction (ORR) catalyst than the undoped CNT and has a good stability toward CO poisoning.[21] In the same work, the theoretical calculations gave the insight of the effects from boron doping at the molecular level. It is found that the boron doping assisted the charge transfer from the carbon nanotube π network to oxygen molecule. The transferred charges weakened the O−O bond and facilitated the adsorption of the oxygen molecule, which is the initial step in ORR reaction. The results from this study indicated the potential of the boron doping to

Received: November 28, 2012
Revised: July 26, 2013
Published: July 30, 2013

   dx.doi.org/10.1021/jp404079j | J. Phys. Chem. C 2013, 117, 17485−17492

activate the oxygen molecule on CNT, which might be useful in ODH reaction, too. This prompts us to investigate the effects from the boron doping on the ODH reactions for nanostructured carbon catalysts. However, the active oxygen functional group in ODH on nanostructured carbon catalyst is generally accepted to be carbonyl group rather than the adsorbed oxygen molecule.[3,8,9,15] It is more relevant to examine the dissociated oxygen molecule on CNT for the reactive oxygen species.

Taking all these considerations into account, the activation of oxygen molecule is studied on boron-doped single-walled carbon nanotube (BSWCNT) without or with a monovacancy defect. The focus is put on the dissociated adsorption of the oxygen molecule, and a periodic (8,8) BSWCNT is used in the simulation. In catalysis, the defects on metal or metal oxide catalyst surfaces are often deemed as the active sites in chemical reactions.[26−28] The inclusion of the vacancy will probably shed light on the possible role played by defects for CNT catalyst, and the monovacancy is one of the common observed defects on CNT.[29] The various structures of dissociated oxygen molecule are explored, and the barrier of the oxygen dissociation is estimated. These calculations will suggest not only how thermodynamically but also kinetically feasible the oxygen molecule activation is on BSWCNT. Furthermore, we propose that the activated oxygen molecule on BSWCNT has the potential to be active sites in the chemical reaction. To test this hypothesis, the partial oxidation of the methane molecule is selected for the evaluation. In most cases, the activation of the short alkane starts from the cleavage of the first C−H. The methane molecule has the most strong C−H bond among the short alkane and the study of the C−H breaking in methane molecule will be informative to the other alkanes. After the first C−H bond breaking, the resulted methyl radical has two different pathways. It can go into the gas phase, which is an entropy-driven process, or it will rebound with the catalyst, mostly binding to the oxygens to form methoxy species.[30,31] The methoxy on the surfaces can further be oxidized to the various products of partial oxidation products of methane-like syngas, CH_3OH, and CH_2O.[32−35] In this study, the pathway leading to formaldehyde is explored, and the reaction barrier is estimated. The results from the calculations will be a useful indicator to the potentials of the BSWCNT as catalyst in the future applications.

2. COMPUTATIONAL METHODS

The calculations reported here are performed by using periodic, spin-polarized DFT as implemented in Vienna ab initio program package (VASP).[36,37] The electron−ion interactions are described by the projector augmented wave (PAW) method proposed by Blöch[38] and implemented by Kresse.[39] PBE functional[40] is used as the exchange-correlation functional approximation, and a plane wave basis set with an energy cutoff of 400 eV is used. Only the gamma point is used in brillouin zone sampling. The (8,8) BSWCNT is placed in a 25.85 × 25.85 × 12.30 Å cell for x, y, z dimension, and the periodic condition is employed along the z direction. The space between neighboring image is 15 Å for x, y dimension, which is enough to exclude the interactions between images. During structure optimization, all atoms in the unit cell are allowed to relax, and no symmetry is imposed. The optimization is stopped when the maximum force on the atoms is smaller than 0.02 eV/Å. The barriers of the activation of oxygen and methane molecules are estimated by using the climbing image nudged elastic band (CI-NEB) method.[41]

The dissociation energy of oxygen molecule is calculated by

$$E_d = E_{O_2/BSWCNT} - E_{O_2} - E_{BSWCNT}$$

where E_d is the dissociation energy of oxygen molecule. The $E_{O_2/BSWCNT}$, E_{O_2}, and E_{BSWCNT} is the total energy of the oxygen molecule on BSWCNT, oxygen molecule in gas phase with triplet ground state, and clean BSWCNT without oxygen molecule, respectively.

3. RESULTS AND DISCUSSIONS

3.1. Boron-Doped Single-Walled Carbon Nanotubes. In current work, only substitutional doping of boron is considered, which means that one of the carbon atoms is replaced by the boron. The optimized structure of boron-doped (8,8) SWCNT is shown in Figure 1. The bond distance

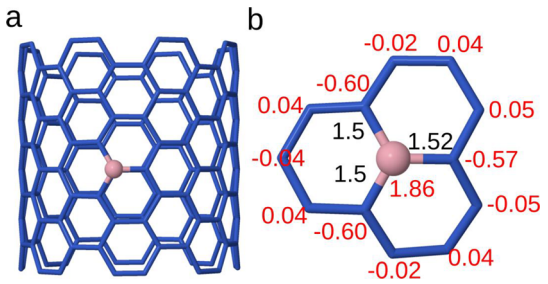

Figure 1. (a) Optimized structure of (8,8) BSWCNT. (b) Bond distance between boron and the neighboring carbons atoms (black, in Å) and the charges (red, e). The blue stick represents carbon, and pink ball represents boron.

between boron and carbon elongates from the C−C distance of 1.42 Å to 1.5 and 1.52 Å after doping. Bader charge analysis[42] shows that each of the three carbon atoms nearest to boron obtains around 0.6 e charges from boron, and boron itself becomes positively charged by 1.86 e. This charge transfer can be understood considering their electronegativity difference, which boron is 2.04 and carbon is 2.55, respectively. When boron took the position that carbon previously occupied, the charges transferred from boron to the neighboring carbons due to carbon's stronger electrophilic ability.

The boron doping also cause the changes in electronic structure of SWCNT. As boron has one less valence electron than carbon, the doping of boron resembles a p-type doping in the semiconductor. The density of states (DOS) of undoped and (8,8) BSWCNT are shown in Figure 2a,b. For undoped (8,8) SWCNT, it is metallic and the valence band makes contact with the bottom of the conduction band. After boron doping, the Fermi level cuts through the top of valence band as shown in Figure 2b,e. In other words, boron doping creates a hole in the (8,8) SWCNT valence band. Furthermore, the splitting at the Fermi level is also observed in the PDOS of the boron and its three neighboring carbons as shown in Figure 2c,d. This electron depletion can also be seen from the electron localization function (ELF) analysis[43] as shown in Figure 2e. ELF is defined between 0 to 1 and the dense localized electrons correspond to the bigger number. So ELF clearly shows the low electron density in the region where boron replaced carbon.

3.2. O_2 Dissociation on Defect-Free BSWCNT. The optimized structures of the dissociated oxygen molecule on

dx.doi.org/10.1021/jp404079j | J. Phys. Chem. C 2013, 117, 17485−17492

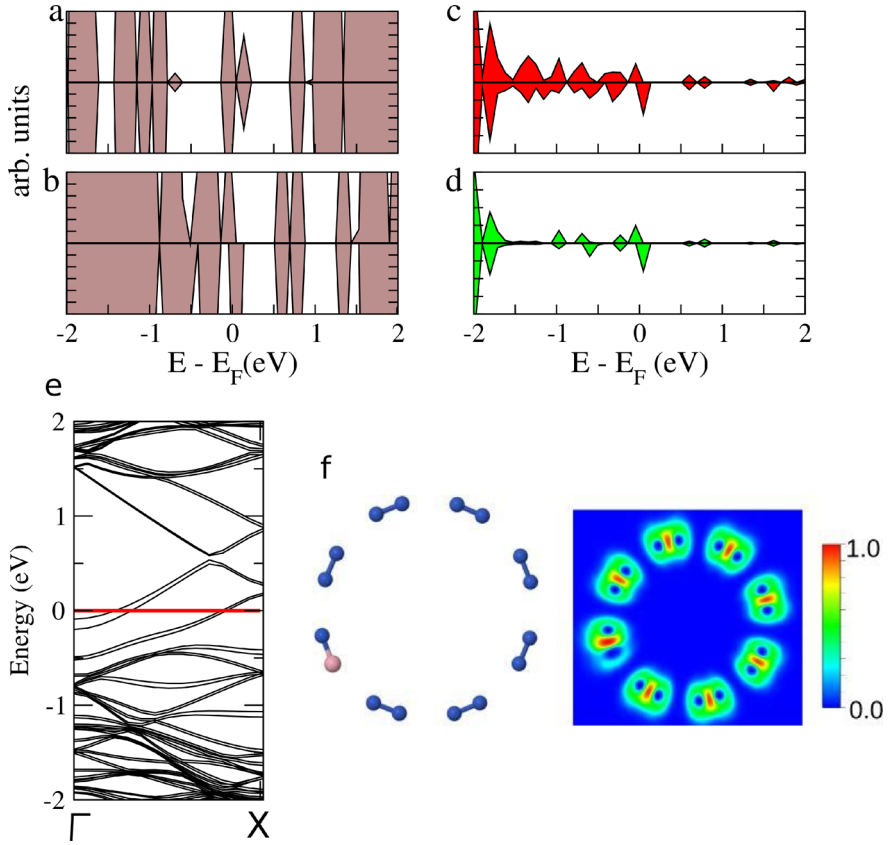

Figure 2. (a) Total density of states (DOS) of undoped (8,8) SWCNT. (b) Total DOS of (8,8) BSWCNT. (c) Partial density of states (PDOS) of three carbons around boron on (8,8) BSWCNT. (d) PDOS of boron on (8,8) BSWCNT. (e) Band structure of (8,8) BSWCNT. The horizontal red line indicates the Fermi level. (f) Electron localization function (ELF) analysis of (8,8) BSWCNT. The plane is cut through the (001) direction. Carbon is blue, and boron is pink.

defect-free BSWCNT are shown in Figure 3a,b. The bond distance in the dissociated oxygen molecule is elongated to 2.35

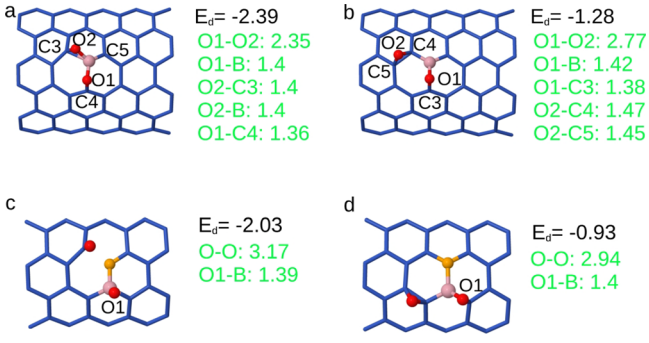

Figure 3. Optimized structures of dissociated oxygen molecule on defect-free (a,b) and defective (c,d) (8,8) BSWCNT. E_d (eV) is the dissociation energy, and the bond distance (Å) is in green. Carbon is blue, oxygen is red, boron is pink, and the oxygen in vacancy is orange.

and 2.77 Å, respectively, for the structures shown in Figure 3a,b, which is far beyond the calculated equilibrium bond distance of 1.23 Å. They indeed corresponded to the dissociated oxygen molecule on BSWCNT. The dissociation energies are −2.39 and −1.28 eV, respectively, and all are exothermic. Inspecting the structure shown in Figure 3a, the dissociated oxygen atoms bridge between boron and its neighboring carbons. The bond distances are all around 1.4 Å. Further, the dissociated oxygen molecule grabbed a total charge of 2.53 *e* and became negatively charged. These charges obtained by oxygens are mainly from two of the three carbons (labeled as C3 and C4 in Figure 3a) nearest to boron, which is involved in the bonding. The reduction of charges on those two carbons, boron, and the third carbon (labeled as C5 in Figure 3a) is 2.18, 0.17, and 0.05 *e*, respectively. The amount of the transferred charge is much larger than the one obtained by the adsorbed oxygen molecule on (5,5) BSWCNT, which is calculated to be 0.45 *e*, and the bond distance in the adsorbed molecule is only 1.32 Å.[21] The difference is understood as the charges obtained by the oxygen molecule go to the antibonding π^* orbital, and the O−O bond is elongated and broken with the increasing obtained charges.[44] For both adsorption and dissociation of the oxygen molecule, the boron atom does not lose charges and acts as a bridge for the charges transferred from BSWCNT to the oxygen molecule. Also, these two carbon atoms (labeled as C3 and C4 in Figure 3a) became positively charged after losing charges to oxygen molecule. It is reasonable to see that the dissociated negatively charged oxygen atoms sit between boron, and these two carbons, which are both positively charged.

The dissociation energy of structure shown in Figure 3b is −1.28 eV and much smaller than the structure shown in Figure 3a. The charges obtained by the dissociated oxygen molecule is −2.10 *e* and is less than the counterpart of structure in Figure 3a, too. The different dissociation sites likely lead to the difference in the calculated dissociation energies. For the structure in Figure 3a, both of the dissociated oxygen atoms are at the positively charged sites. However, for structure in Figure

dx.doi.org/10.1021/jp404079j | J. Phys. Chem. C 2013, 117, 17485−17492

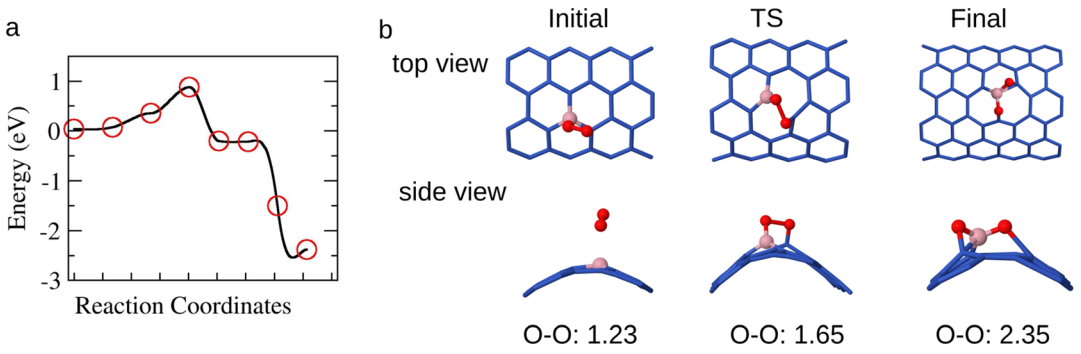

Figure 4. (a) MEP of the oxygen dissociation on (8,8) BSWCNT. (b) Structures of the initial, transition state (TS), and final state on MEP. The bond distance between the dissociated oxygen molecule is in Å. Carbon is blue, oxygen is red, and boron is pink.

3b, one of the dissociated oxygen atoms (labeled as O2) bridges between the nearest carbon to boron (labeled as C4) and second nearest carbon (labeled as C5), which are negatively and positively charged, respectively.

For the structure in Figure 3a, the climbing nudged elastic band theory calculations (CI-NEB) are carried out to study the minimum energy path (MEP) and estimate the dissociation barrier. The MEP of the oxygen molecule dissociation is shown in Figure 4a, and the barrier is estimated to be 0.88 eV. The structures of the initial, transition state (TS), and final state are also included in Figure 4b. Initially, the oxygen molecule is in gas phase with the O−O bond distance of 1.23 Å. At transition state, the O−O bond distance elongated to be 1.65 Å and the oxygen atoms bind to boron and its nearest carbon with the bond distance of 1.34 and 1.39 Å, respectively. The charges on the O_2 molecule in TS is 1.40 *e*. After transition state, the bond between two oxygen atoms is completely broken and the final state is reached. It is necessary to point out the barrier from current work is comparable with the one on nitrogen-doped SWCNT of 0.86 eV from DFT calculations.[45]

3.3. O_2 Dissociation at Monovacancy on BSWCNT. In general, defective sites including steps and vacancies are believed to be chemical active sites in reactions on metal and metal oxide catalyst surfaces.[26−28] There are also some theoretical and experimental works suggesting the importance played by defects in reactions on carbon-based material.[46−48] Here, we want to understand the possible influence from the monovacancy on the activation of oxygen molecule.

The optimized structure of BSWCNT with a monovacancy (vBSWCNT) is shown in Figure 5. Compared with initial structure, boron atom has a tendency to keep bonding with three carbons at vacancy after optimization. This leads to one carbon atom (c in Figure 5) at a vacancy moving toward boron and building a bond of 1.72 Å with boron after optimization,

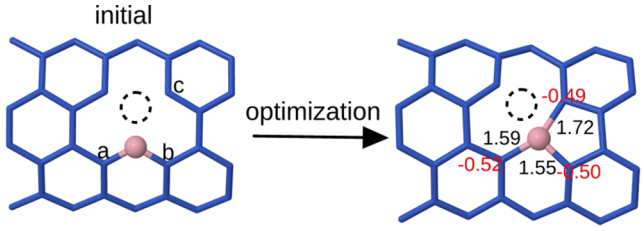

Figure 5. Initial and optimized structures of a monovacancy on (8,8) BSWCNT. The black dashed circle indicates the missing carbon atom. The black and red numbers are bond distance (Å) and charges (*e*), respectively.

and the other two carbons (a,b) have bond distances of 1.59 and 1.55 Å with boron, respectively. It is noted that all three bond distances become longer than the counterparts on vacancy-free BSWCNT. This elongated bond comes with the less charges obtained by the three carbons around boron. The total charges of these three carbons is −1.51 *e* and 0.26 less than the vacancy-free BSWCNT.

We carry out the CI-NEB calculations to study the interaction between O_2 molecule and monovacancy defect. From the MEP plot shown in Figure 6a, the dissociation of O_2 molecule at vacancy is a barrierless process. For the structure of the final state as shown in Figure 6b, one of the dissociated oxygen atoms fills in the vacancy site and another one bonds to a carbon atom. The structure is quite stable as the inserted oxygen forms a covalent bond with the neighboring carbon and boron as shown in Figure 6c. Further, the larger exothermic energy was also observed for the CO dissociation at the vacancy site on graphite(0001), which the vacancy site is filled by the carbon atom and the process is exothermic by −4.82 eV.[49] When interacting with the oxidant, the monovacancy on BSWCNT is easily oxidized. Therefore, the discussions on the property of monovacancy in an oxidizing environment are necessary to start with the structure of the filled vacancy with the oxygen atom.

The structures of the dissociated oxygen molecule on vBSWCNT are presented in Figure 3c,d. The dissociation energies are −2.03 and −0.93 eV, respectively. The exothermic dissociation energies indicate that the vBSWCNT with the filled vacancy is still thermodynamically capable of breaking a O−O bond. For the structure shown in Figure 3c, which has larger dissociation energy, the barrier of the oxygen dissociation is estimated to be 0.12 eV as shown in Figure 7a. Notably, the barrier is much smaller than the one on defect-free BSWCNT. The important structures on MEP are shown in Figure 7b. Similar to the MEP on defect-free BSWCNT, the dissociation starts from the oxygen molecule in the gas phase. The structure of TS is more like the initial state, and the bond distance is extended to 1.35 Å with the obtained charges of 0.40 *e* on the two oxygen atoms. It is evident that the TS on vBSWCNT is an early transition state, while it is more like the final state on defect-free BSWCNT. Moreover, a shorter O−O bond distance and the less charges obtained by oxygen molecule for TS on vBSWCNT are witnessed compared to the defect-free BSWCNT. The monovacancy site on vBSWCNT shows a better ability to activate an oxygen molecule, and the calculations indicate the important role played by defective sites.

dx.doi.org/10.1021/jp404079j | J. Phys. Chem. C 2013, 117, 17485−17492

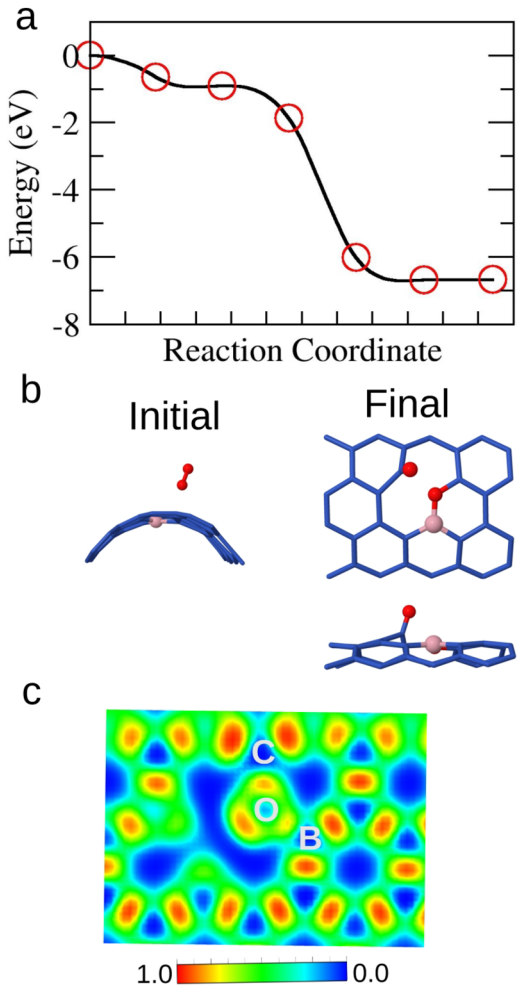

Figure 6. (a) MEP of oxygen molecule dissociation on (8,8) vBSWCNT. (b) Initial and final structures on the reaction path. (c) ELF of the final structure, which indicates the covalent bond between inserted oxygen atom and boron, carbon. Carbon is blue, oxygen is red, and boron is pink.

3.4. CH_4 Activation on BSWCNT. From the above calculations, the BSWCNT demonstrate the ability to activate the oxygen molecule especially at a defective vacancy site. The next issue we aim to address is whether the oxygen species on BSWCNT have any effects on the ODH reaction. More specific, can they be the active sites to break the C−H bond in alkane molecules. For this end, the methane molecule is selected for the test, and the breaking of the first C−H bond is examined.

The dissociative adsorption of methane molecule is studied on the structures shown in Figure 3a,c. The dissociated fragments bind to the oxygens on BSWCNT to form hydroxyl and methoxide, respectively, as shown in the final structures in Figures 8 and 9. The barrier for the methane dissociation is estimated, and the MEPs are shown in Figures 8 and 9. At first glance, the two MEPs look quite similar for defect-free and defective BSWCNT as they both have a terrace on MEP after the transition state. However, the barrier is different, which is 1.45 and 0.95 eV, respectively, for defect-free and defective BSWCNT. On both MEPs, initially, methane molecule is in the gas phase and moving toward the BSWCNT. There is a rapid rise in energy along with the breaking of the C−H bond until TS is reached. For TS structures, the C−H bond is completely broken, and the bond distances are 1.84 and 2.34 Å, respectively.

The charge analysis is carried out for TS structures of methane dissociation and listed in Table 1. For TS structure on defect-free BSWCNT, which is shown in Figure 8, the charge on the hydrogen atom, which forms the surface hydroxyl, is reduced to 0.35 *e* from 0.95 *e* in gas phase methane molecule, and the methyl radical has the charge of 6.98 *e*, which experiences a very small variation compared with the initial state. However, the charge on the carbon atom (labeled as C3 in Figure 8) is increased to 3.95 *e* from 3.56 *e* before the methane dissociation, while the charges on oxygen, which forms hydroxyl, is slightly increased by 0.1 *e*, and boron is nearly unchanged. The similar reduction of charge on hydrogen is also observed for Pd-doped ceria for methane activation.[50] The analysis shows that the breaking of C−H bond results from the charge abstraction from hydrogen to the BSWCNT. The acceptor on BSWCNT is not oxygen, which forms hydroxyl, but the carbon atom, which is used to bond to oxygen before methane dissociation. For the TS structure on vBSWCNT shown in Figure 9, the methane molecule is still dissociated into a methyl radical and a surface hydroxyl. The charge on the hydrogen in hydroxyl is only 0.38 *e*, which has a reduction of 0.57 *e* from the gas phase methane molecule. However, the charge acceptor on vBSWCNT is oxygen rather than the carbon atom. The charge of the oxygen, which forms hydroxyl, increases to be 7.35 *e* from 6.89 *e* before methane dissociation. It is noted that the charge of the oxygen forming hydroxyl in TS structure on BSWCNT in Figure 8 is already 7.25 *e* even before interacting with the methane molecule, which limits its ability to accommodate more charges.

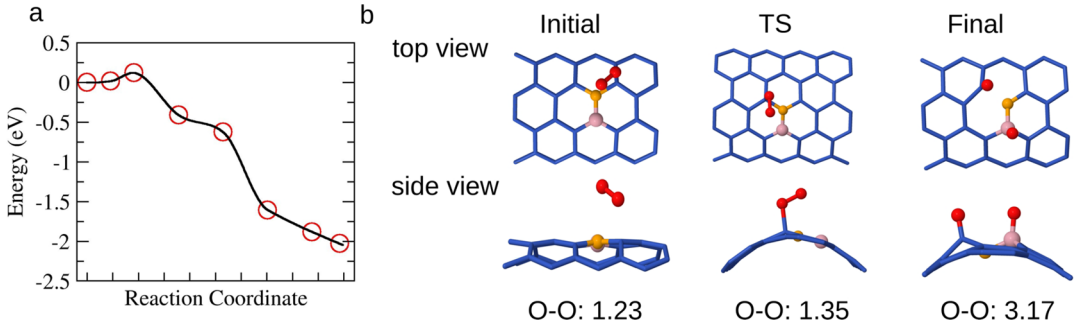

Figure 7. (a) MEP of the oxygen dissociation on vBSWCNT with the oxygen atom filling in the vacancy. (b) Structures of the initial, transition state (TS), and final state on MEP. The bond distance between the dissociated oxygen moelcule is in Å. Carbon is blue, oxygen is red, boron is pink, and the oxygen filling vacancy is orange.

dx.doi.org/10.1021/jp404079j | J. Phys. Chem. C 2013, 117, 17485−17492

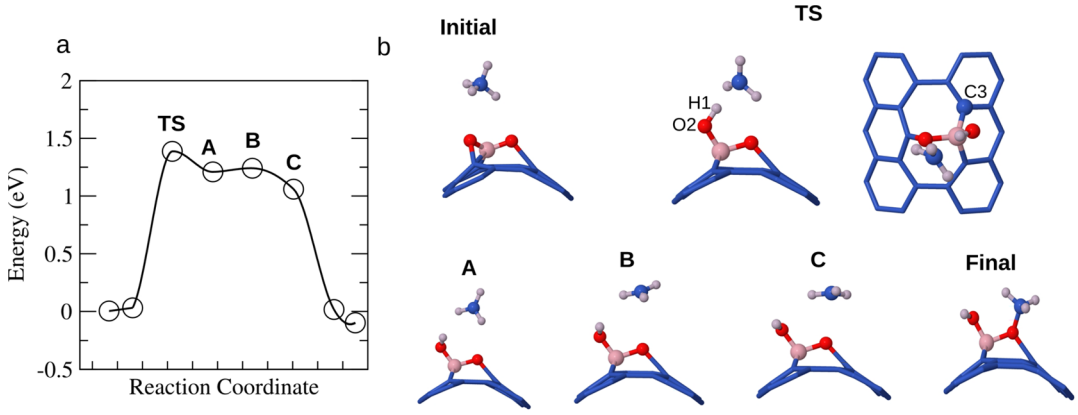

Figure 8. (a) MEP of the methane activation on (8,8) BSWCNT. (b) Structures along the MEP. Carbon is blue, oxygen is red, boron is pink, and hydrogen is white.

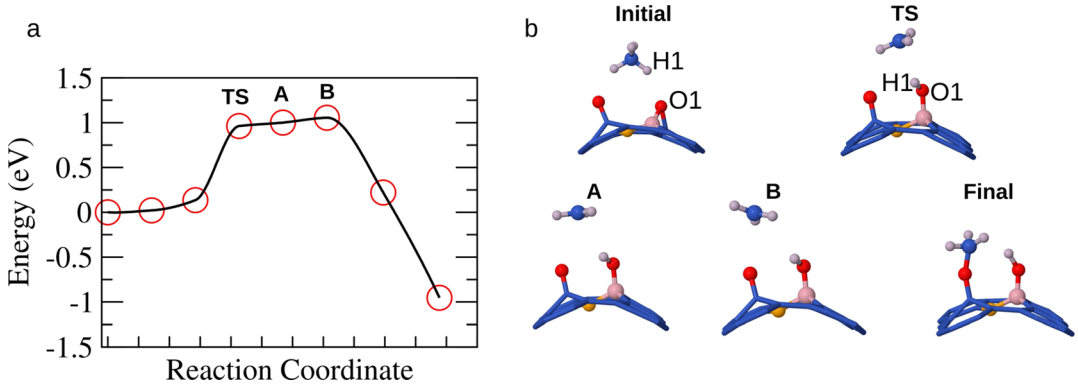

Figure 9. (a) MEP of the methane activation on (8,8) vBSWCNT with the oxygen filling in the vacancy. (b) Structures along the MEP. Carbon is blue, oxygen is red, boron is pink, hydrogen is white, and the oxygen filling vacancy is orange.

Table 1. Charges on the Atoms in TS Structures As Shown in Figure 8 and 9[a]

	O2	C3	boron	H1	methyl group
TS in Figure 8	7.35	3.95	0.96	0.35	6.98
reference (initial)	7.25	3.56	0.97	0.95	7.05
	O1		boron	H1	methyl group
TS in Figure 9	7.35		0.94	0.38	6.98
reference (initial)	6.89		0.98	0.95	7.05

[a]The labels are indicated in the corresponding figures. The charge of atoms on BSWCNT and vBSWCNT in initial structures is also listed as a reference.

Staring from TS, there is a terrace on both MEPs, which is corresponding to the movement of methyl radical to reach its adsorption site as shown as a series structures on MEP (A, B, and C in Figure 8 and A and B in Figure 9). The energy plummets once the methyl radical binds the oxygen on BSWCNT. The similar feature of MEP has been observed for the methane activation on Pd-doped ceria.[50] For Pd-doped ceria catalyst, the terrace region is also related to the methyl radical movement. This observation gives an evidence of the similarity between the CNT catalyst and the metal oxide catalyst, which has been discussed before.[17]

3.5. CH_3 Oxidation to Formaldehyde. As mentioned before, the resulting CH_3 on BSWCNT can further be converted to the various products of the partial oxidation of methane. Here, the reaction path and the barrier to the formaldehyde on BSWCNT are investigated. The initial, transition, and final states along the reaction coordinate are shown in Figure 10. Starting from the final structure shown in Figure 8, there are the CH_3 group and the hydroxyl on BSWCNT after the first C−H bond breaking. The hydrogen in CH_3 can be further abstracted by the neighboring oxygen, which leads to the formation of the formaldehyde and water.

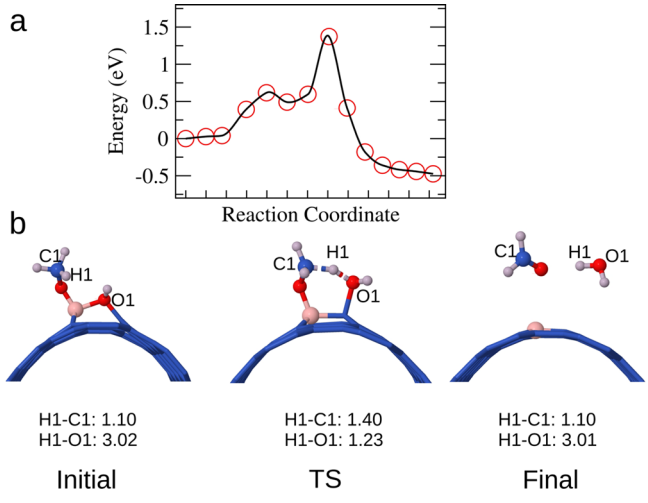

Figure 10. (a) MEP of the conversion of CH_3 to formaldehyde on (8,8) BSWCNT. (b) Structures of initial, transition state (TS), and final states on the MEP. The bond distance is in Å and black. Carbon is blue, oxygen is red, boron is pink, and the hydrogen is white.

dx.doi.org/10.1021/jp404079j | J. Phys. Chem. C 2013, 117, 17485−17492

Along the reaction coordinate as shown in Figure 10, the CH_3 and the neighboring oxygen are approaching each other. At the transition state, the bond distance is 1.40 and 1.23 Å, respectively, for the hydrogen, which is the one breaking off from CH_3 (H1 in Figure 10), with the carbon in CH_3 group (C1 in Figure 10), and the oxygen in the neighboring hydroxyl (O1 in Figure 10). Compared with the bond distance in the initial structure, it is obvious that the C−H is stretched, and the O−H bond is forming. The barrier of this process is estimated to be 1.37 eV, which is comparable to the first C−H bond breaking in methane molecule. After the transition state, the formaldehyde and water molecules are formed and leave from the BSWCNT.

4. SUMMARY

In current work, the DFT calculations are carried out to study the dissociation of oxygen molecule on defect-free and defective boron-doped SWCNT and their role in the activation of the methane molecule. The boron doping causes the charges to be transferred from boron to neighboring carbons, and the splitting at Fermi level creates a hole in the valence band. It is observed that the charges from the carbons around boron transferred to the dissociated oxygen molecule break the O−O bond, and the favorite adsorption site are these positively charged atoms on BSWCNT. The barrier of the oxygen molecule activation on defect-free BSWCNT is 0.88 eV. For the oxygen molecule dissociation on vBSWCNT, it is found that the vacancy site is easily oxidized and that the oxidized structure is quite stable. The barrier on vBSWCNT is 0.12 eV, much smaller than the defect-free BSWCNT, which is a reminder of the importance of the defective site.

The catalytic property of the dissociated oxygen molecule on BSWCNT and vBSWCNT is further tested for the C−H bond breaking in methane molecule and the partial oxidation to the formaldehyde. The broken C−H bond in methane molecule results from the charge abstraction from hydrogen in methane molecule to the catalyst. After the transition state, there is a terrace on MEP that corresponds to the movement of methyl radical to the adsorption site. Interestingly, the phenomena is also observed for the Pd-doped ceria catalyst.[50] The barrier of the methane activation is 1.45 and 0.95 eV, respectively, for defect-free and defective BSWCNT. The barriers are comparable with other catalysts. For example, the barrier of Pd-doped ceria and nitrogen-doped CNT is 1.08 and 1.12 eV, respectively.[50,51]

The CH_3 groups resulting from the first C−H bond dissociation can further be oxidized to formaldehyde. One of the hydrogens in CH_3 group is abstracted by the neighboring oxygen, which leads to the formation of the formaldehyde and water molecule. With the desorption of the products, formaldehyde and water, the catalyst changes back to its initial state and a catalytic cycle is completed. Overall, the calculations show that boron doping is an alternative way to adjust the properties of CNT catalyst in chemical reactions.

AUTHOR INFORMATION

Corresponding Author

*(D.S.) E-mail: dangsheng@fhi-berlin.mpg.de.

Notes

The authors declare no competing financial interest.

ACKNOWLEDGMENTS

B.L. is supported by SYNL-T.S. K̂ Research Fellowship. B.L. is thankful for the financial grant from the China Postdoctoral Science Foundation (2012M511186) and computing time from ShenYang Branch, Supercomputing Center of CAS. This work is also supported by NSFC (21133010) and MOST (2011CBA00504).

REFERENCES

(1) Serp, P.; Castillejos, E. Catalysis in Carbon Nanotubes. *ChemCatChem* **2010**, *2*, 41−47.

(2) Delgado, J.; Su, D.; Rebmann, G.; Keller, N.; Gajović, A.; Schlögl, R. Immobilized Carbon Nanofibers As Industrial Catalyst for ODH Reactions. *J. Catal.* **2006**, *244*, 126−129.

(3) Sui, Z.-J.; Zhou, J.-H.; Dai, Y.-C.; Yuan, W.-K. Oxidative Dehydrogenation of Propane over Catalysts Based on Carbon Nanofibers. *Catal. Today* **2005**, *106*, 90−94.

(4) Zhang, J.; Su, D. S.; Blume, R.; Schlögl, R.; Wang, R.; Yang, X.; Gajović, A. Surface Chemistry and Catalytic Reactivity of a Nanodiamond in the Steam-Free Dehydrogenation of Ethylbenzene. *Angew. Chem., Int. Ed.* **2010**, *49*, 8640−8644.

(5) Machado, B. F.; Serp, P. Graphene-Based Materials for Catalysis. *Catal. Sci. Technol.* **2012**, *2*, 54−75.

(6) Frank, B.; Morassutto, M.; Schomäcker, R.; Schlögl, R.; Su, D. Oxidative Dehydrogenation of Ethane over Multiwalled Carbon Nanotubes. *ChemCatChem* **2010**, *2*, 644−648.

(7) Liu, L.; Deng, Q.-F.; Agula, B.; Ren, T.-Z.; Liu, Y.-P.; Zhaorigetu, B.; Yuan, Z.-Y. Synthesis of Ordered Mesoporous Carbon Materials and Their Catalytic Performance in Dehydrogenation of Propane to Propylene. *Catal. Today* **2012**, *186*, 35−41.

(8) Michorczyk, P.; Kuśtrowski, P.; Niebrzydowska, P.; Wach, A. Catalytic Performance of Sucrose-Derived CMK-3 in Oxidative Dehydrogenation of Propane to Propene. *Appl. Catal., A* **2012**, *445−446*, 321−328.

(9) Zhang, J.; Liu, X.; Blume, R.; Zhang, A.; Schlögl, R.; Su, D. S. Surface-Modified Carbon Nanotubes Catalyze Oxidative Dehydrogenation of *n*-Butane. *Science* **2008**, *322*, 73−77.

(10) Liang, C.; Xie, H.; Schwartz, V.; Howe, J.; Dai, S.; Overbury, S. H. Open-Cage Fullerene-Like Graphitic Carbons As Catalysts for Oxidative Dehydrogenation of Isobutane. *J. Am. Chem. Soc.* **2009**, *131*, 7735−7741.

(11) Liu, X.; Frank, B.; Zhang, W.; Cotter, T. P.; Schlögl, R.; Su, D. S. Carbon-Catalyzed Oxidative Dehydrogenation of *n*-Butane: Selective Site Formation during sp^3-to-sp^2 Lattice Rearrangement. *Angew. Chem., Int. Ed.* **2011**, *50*, 3318−3322.

(12) Keller, N.; Maksimova, N.; Roddatis, V.; Schur, M.; Mestl, G.; Butenko, Y.; Kuznetsov, V.; Schlögl, R. The Catalytic Use of Onion-Like Carbon Materials for Styrene Synthesis by Oxidative Dehydrogenation of Ethylbenzene. *Angew. Chem., Int. Ed.* **2002**, *41*, 1885.

(13) Pereira, M. F. R.; Figueiredo, J. L.; Órfão, J. J.; Serp, P.; Kalck, P.; Kihn, Y. Catalytic Activity of Carbon Nanotubes in the Oxidative Dehydrogenation of Ethylbenzene. *Carbon* **2004**, *42*, 2807−2813.

(14) Qui, N.; Scholz, P.; Krech, T.; Keller, T.; Pollok, K.; Ondruschka, B. Multiwalled Carbon Nanotubes Oxidized by UV/H_2O_2 As Catalyst for Oxidative Dehydrogenation of Ethylbenzene. *Catal. Commun.* **2011**, *12*, 464−469.

(15) Macia-Agullo, J. A.; Cazorla-Amoros, D.; Linares-Solano, A.; Wild, U.; Su, D. S.; Schlögl, R. Oxygen Functional Groups Involved in the Styrene Production Reaction Detected by Quasi in Situ XPS. *Catal. Today* **2005**, *102*, 248−253.

(16) Yu, D.; Nagelli, E.; Du, F.; Dai, L. Metal-Free Carbon Nanomaterials Become More Active than Metal Catalysts and Last Longer. *J. Phys. Chem. Lett.* **2010**, *1*, 2165−2173.

(17) Su, D. S.; Zhang, J.; Frank, B.; Thomas, A.; Wang, X.; Paraknowitsch, J.; Schlögl, R. Metal-Free Heterogeneous Catalysis for Sustainable Chemistry. *ChemSusChem* **2010**, *3*, 169−180.

(18) Bitter, J. H. Nanostructured Carbons in Catalysis a Janus Material-Industrial Applicability and Fundamental Insights. *J. Mater. Chem.* **2010**, *20*, 7312−7321.
(19) Figueiredo, J. L.; Pereira, M. F. R. The Role of Surface Chemistry in Catalysis with Carbons. *Catal. Today* **2010**, *150*, 2−7.
(20) Haruyama, J. Novel Quantum Phenomena in Carbon Nanotubes; Superconductivity, One-Dimensional Electron Correlations, and Spin Quantum Bits. *J. Comput. Theor. Nanosci.* **2010**, *7*, 1688−1706.
(21) Yang, L.; Jiang, S.; Zhao, Y.; Zhu, L.; Chen, S.; Wang, X.; Wu, Q.; Ma, J.; Ma, Y.; Hu, Z. Boron-Doped Carbon Nanotubes as Metal-Free Electrocatalysts for the Oxygen Reduction Reaction. *Angew. Chem., Int. Ed.* **2011**, *50*, 7132−7135.
(22) Talla, J. A. First Principles Modeling of Boron-Doped Carbon Nanotube Sensors. *Phys. B* **2012**, *407*, 966−970.
(23) Bai, L.; Zhou, Z. Computational Study of B- or N-Doped Single-Walled Carbon Nanotubes As NH_3 and NO_2 Sensors. *Carbon* **2007**, *45*, 2105−2110.
(24) Sankaran, M.; Viswanathan, B. Hydrogen Storage in Boron Substituted Carbon Nanotubes. *Carbon* **2007**, *45*, 1628−1635.
(25) Kuchta, B.; Firlej, L.; Roszak, S.; Pfeifer, P. A Review of Boron Enhanced Nanoporous Carbons for Hydrogen Adsorption: Numerical Perspective. *Adsorption* **2010**, *16*, 413−421.
(26) Liu, Z. P.; Hu, P. General Rules for Predicting Where a Catalytic Reaction Should Occur on Metal Surfaces: A Density Functional Theory Study of C−H and C−O Bond Breaking/Making on Flat, Stepped, and Kinked Metal Surfaces. *J. Am. Chem. Soc.* **2003**, *125*, 1958−1967.
(27) Pacchioni, G. Oxygen Vacancy: The Invisible Agent on Oxide Surfaces. *ChemPhysChem* **2003**, *4*, 1041−1047.
(28) Wu, X.; Selloni, A.; Lazzeri, M.; Nayak, S. K. Oxygen Vacancy Mediated Adsorption and Reactions of Molecular Oxygen on the TiO_2(110) Surface. *Phys. Rev. B* **2003**, *68*, 241402.
(29) Charlier, J.-C. Defects in Carbon Nanotubes. *Acc. Chem. Res.* **2002**, *35*, 1063−1069.
(30) Pitchai, R.; Klier, K. Partial Oxidation of Methane. *Catal. Rev.-Sci. Eng.* **1986**, *28*, 13−88.
(31) Tabata, K.; Teng, Y.; Takemoto, T.; Suzuki, E.; Bañares, M. A.; Peña, M. A.; Fierro, J. L. G. Activation of Methane by Oxygen and Nitrogen Oxides. *Catal. Rev.-Sci. Eng.* **2002**, *44*, 1−58.
(32) Lunsford, J. H. Catalytic Conversion of Methane to More Useful Chemicals and Fuels: a Challenge for the 21st Century. *Catal. Today* **2000**, *63*, 165−174.
(33) Christian Enger, B.; Lødeng, R.; Holmen, A. A Review of Catalytic Partial Oxidation of Methane to Synthesis Gas with Emphasis on Reaction Mechanisms over Transition Metal Catalysts. *Appl. Catal., A* **2008**, *346*, 1−27.
(34) Fierro, J. Catalysis in C1 Chemistry: Future and Prospect. *Catal. Lett.* **1993**, *22*, 67−91.
(35) Herman, R. G.; Sun, Q.; Shi, C.; Klier, K.; Wang, C.-B.; Hu, H.; Wachs, I. E.; Bhasin, M. M. Development of Active Oxide Catalysts for the Direct Oxidation of Methane to Formaldehyde. *Catal. Today* **1997**, *37*, 1−14.
(36) Kresse, G.; Furthmüller, J. Efficiency of ab-Initio Total Energy Calculations for Metals and Semiconductors Using a Plane-Wave Basis Set. *Comput. Matt. Sci.* **1996**, *6*, 15.
(37) Kresse, G.; Furthmüller, J. Efficient Iterative Schemes for ab Initio Total-Energy Calculations Using a Plane-Wave Basis Set. *Phys. Rev. B* **1996**, *54*, 11169.
(38) Blöchl, P. E. Projector Augmented-Wave Method. *Phys. Rev. B* **1994**, *50*, 17953.
(39) Kresse, G.; Joubert, D. From Ultrasoft Pseudopotentials to the Projector Augmented-Wave Method. *Phys. Rev. B* **1999**, *59*, 1758.
(40) Perdew, J. P.; Burke, K.; Ernzerhof, M. Generalized Gradient Approximation Made Simple. *Phys. Rev. Lett.* **1996**, *77*, 3865−3868.
(41) Henkelman, G.; Uberuaga, B. P.; Jonsson, H. A Climbing Image Nudged Elastic Band Method for Finding Saddle Points and Minimum Energy Paths. *J. Chem. Phys.* **2000**, *113*, 9901−9904.
(42) Bader, R. *Atoms in Molecules: A Quantum Theory*; Clarendon Press: New York, 1990.
(43) Becke, A. D.; Edgecombe, K. E. A Simple Measure of Electron Localization in Atomic and Molecular Systems. *J. Chem. Phys.* **1990**, *92*, 5397−5403.
(44) Bielański, A.; Haber, J. *Oxygen in Catalysis*; Marcel Dekker Incorporated: New York, 1991.
(45) Ni, S.; Li, Z. Y.; Yang, J. L. Oxygen Molecule Dissociation on Carbon Nanostructures with Different Types of Nitrogen Doping. *Nanoscale* **2012**, *4*, 1184−1189.
(46) Allouche, A.; Ferro, Y. Dissociative Adsorption of Small Molecules at Vacancies on the Graphite Surface. *Carbon* **2006**, *44*, 3320−3327.
(47) Song, S.; Jiang, S.; Rao, R.; Yang, H.; Zhang, A. Bicomponent VO_2-Defects/MWCNT Catalyst for Hydroxylation of Benzene to Phenol: Promoter Effect of Defects on Catalytic Performance. *Appl. Catal., A* **2011**, *401*, 215−219.
(48) Song, S.; Jiang, S. Selective Catalytic Oxidation of Ammonia to Nitrogen over CuO/CNTs: The Promoting Effect of the Defects of CNTs on the Catalytic Activity and Selectivity. *Appl. Catal., B* **2012**, *117−118*, 346−350.
(49) Xu, S. C.; Irle, S.; Musaev, D. G.; Lin, M. C. Quantum Chemical Prediction of Pathways and Rate Constants for Reactions of CO and CO_2 with Vacancy Defects on Graphite (0001) Surfaces. *J. Phys. Chem. C* **2009**, *113*, 18772−18777.
(50) Tang, W.; Hu, Z. P.; Wang, M. J.; Stucky, G. D.; Metiu, H.; McFarland, E. W. Methane Complete and Partial Oxidation Catalyzed by Pt-Doped CeO_2. *J. Catal.* **2010**, *273*, 125−137.
(51) Hu, X.; Zhou, Z.; Lin, Q.; Wu, Y.; Zhang, Z. High Reactivity of Metal-Free Nitrogen-Doped Carbon Nanotube for Nanotube the C−H Activation. *Chem. Phys. Lett.* **2011**, *503*, 287−291.